Energy Absorption of Thin-Walled Square Tubes With a Prefolded Origami Pattern—Part I: Geometry and Numerical Simulation

Article *in* Journal of Applied Mechanics · August 2013

DOI: 10.1115/1.4024405

1 author:

Jiayao Ma
University of Oxford
55 PUBLICATIONS **320** CITATIONS

Energy Absorption of Thin-Walled Square Tubes With a Prefolded Origami Pattern—Part I: Geometry and Numerical Simulation

Jiayao Ma

Zhong You[1]
e-mail: zhong.you@eng.ox.ac.uk

Department of Engineering Science,
University of Oxford,
Parks Road,
Oxford OX1 3PJ, UK

Thin-walled tubes subjected to axial crushing have been extensively employed as energy absorption devices in transport vehicles. Conventionally, they have a square or rectangular section, either straight or tapered. Dents are sometimes added to the surface in order to reduce the initial buckling force. This paper presents a novel thin-walled energy absorption device known as the origami crash box that is made from a thin-walled tube of square cross section whose surface is prefolded according to a developable origami pattern. The prefolded surface serves both as a type of geometric imperfection to lower the initial buckling force and as a mode inducer to trigger a collapse mode that is more efficient in terms of energy absorption. It has been found out from quasi-static numerical simulation that a new collapse mode referred to as the completed diamond mode, which features doubled traveling plastic hinge lines compared with those in conventional square tubes, can be triggered, leading to higher energy absorption and lower peak force than those of conventional ones of identical weight. A parametric study indicates that for a wide range of geometric parameters the origami crash box exhibits predictable and stable collapse behavior, with an energy absorption increase of 92.1% being achieved in the optimum case. The origami crash box can be stamped out of a thin sheet of material like conventional energy absorption devices without incurring in-plane stretching due to the developable surface of the origami pattern. The manufacturing cost is comparable to that of existing thin-walled crash boxes, but it absorbs a great deal more energy during a collision. [DOI: 10.1115/1.4024405]

Keywords: thin-walled tube, energy absorption, axial crushing, origami pattern, developable surface

1 Introduction

In transport vehicle design, an increasing emphasis is put on safety. A common design approach to enhance the crashworthiness of a vehicle is to install energy absorption devices which deform and absorb kinetic energy during a low speed collision. Thin-walled metal tubes, particularly those with a circular or square section, have been widely used for this purpose because of their relatively stable and predictable collapse mode, long stroke, and low costs. In automobiles, the device, also known as the crash box due to its tubular profile with a square or rectangular section, is mounted between the bumper and the main frame of a vehicle to absorb energy in the event of an impact. The primary energy absorbers in trains adopt a similar square tubular form [1]. Circular tubular structures are also found in the landing gears of helicopters [2].

A significant amount of research has been done on the energy absorption characteristics of thin-walled tubes, with both circular and square section subjected to axial crushing. Depending on tube diameter D to wall thickness t ratio, D/t, circular tubes could be crushed in the axis-symmetric concertina mode, the nonsymmetric diamond mode, or a mixture of the two [3]. A great deal of literature on the concertina mode [4–6] and the diamond mode [7–9] are available.

Like circular tubes, square tubes also exhibit various collapse modes depending on tube width b to wall thickness t ratio, b/t. Relatively thin and short square tubes, most commonly used in energy absorption devices, usually collapse in the symmetric mode. Wierzbicki and Abramowicz [10] established a kinematically admissible and circumferentially inextensional basic folding element, also known as super folding element, which consisted of trapezoidal, cylindrical, conical, and toroidal surfaces. Two types of plastic hinge lines, namely, the stationary plastic hinge lines, which stayed in the same place throughout folding, and traveling plastic hinge lines, which transmitted over the thin-walled surfaces as the element collapsed, were considered in the element. The study showed that the energy dissipation of the element came from three main sources, i.e., folding along stationary plastic hinge lines, propagation of traveling plastic hinge lines, and localized in-plane stretching in the toroidal surface which was associated with traveling plastic hinge lines in order to satisfy the condition of kinematical continuity of the element. An important conclusion drawn from the study was that traveling plastic hinge lines, which accounted for two-thirds of the total energy absorption caused by the propagation of themselves and the associated in-plane stretching, were most effective at dissipating energy. Abramowicz and Jones [11,12] further modified the element by introducing the concept of effective crushing distance and derived the theoretical expression for the mean crushing force as follows:

$$P_m = 13.06\sigma_0 b^{1/3} t^{5/3} \quad (1)$$

[1]Corresponding author.

Contributed by the Applied Mechanics Division of ASME for publication in the Journal of Applied Mechanics. Manuscript received September 21, 2012; final manuscript received March 5, 2013; accepted manuscript posted May 7, 2013; published online August 22, 2013. Assoc. Editor: Glaucio H. Paulino.

in which σ_0 is equivalent plastic flow stress. For elastic-strain hardening materials with power law hardening behavior, σ_0 can be calculated by Ref. [13]

$$\sigma_0 = \sqrt{\frac{\sigma_y \sigma_u}{1+n}} \tag{2}$$

where σ_y is yield stress, σ_u is tensile strength, and n is power law exponent.

Thick square tubes fail in the extensional mode. This mode involves large material in-plane extension in the circumferential direction and folding along stationary plastic hinge lines. The mean crushing force can be estimated as Ref. [14]

$$P_m = 8.16\sigma_0 t^{3/2} b^{1/2} + 2.04\sigma_0 t^2 \tag{3}$$

The mean crushing force associated with the extensional mode is higher than that with the symmetric mode for b/t values higher than 7.5, indicating that circumferential membrane deformation requires much more energy to be activated than bending in thin tubes with b/t much larger than 7.5. This further explains why commonly used thin-walled square tubes as energy absorption devices tend to assume a circumferentially inextensional collapse mode.

An ideal energy absorption device should satisfy the following twin conditions. First, it must have a low peak force, i.e., the highest reaction force during the crushing process, in order that no excessive force is transmitted to the main structure it is designed to protect. Secondly, the mean crushing force, defined as the total energy absorption divided by the final crushing distance, needs to be high to dissipate as much kinetic energy as possible [3]. A commonly adopted approach to reduce the peak force is to introduce dents at predetermined locations on the surface of a tube. Relevant research includes the work done by Singace and El-Sobky [15] and Hosseinipour and Daneshi [16] on circular tubes, and by Lee et al. [17] on square tubes. With respect to increasing the mean crushing force, Adachi et al. [18] applied circumferential ribs as stiffeners to reduce the longitudinal wavelength of circular tubes and reported as much as 30% increase in mean crushing force. Lee et al. [19] used a controller to improve the energy absorption of square tubes and reported about 15–20% increase in mean crushing force. For actual crash boxes used in automotive industry, dents or even patterns are stamped out on the surface of thin-walled boxes in order to reduce the peak force while maintaining the collapse mode, which is in fact the symmetric mode of a thin-walled square tube even if the load is slightly eccentric. An interesting attempt to achieve both objectives within a design is to introduce a type of pyramid pattern on the surface of a square tube [20]. However, experimental results revealed that the tube with pyramid pattern was very sensitive to imperfections and the expected octagonal mode was not always triggered [21]. Moreover, the pyramid pattern is nondevelopable and hence, the conventional stamping method may lead to large in-plane deformation.

In this paper, we propose a novel energy absorption device referred to as the origami crash box hereafter. It uses a specifically designed developable origami pattern to prefold the thin-walled surface with the aim to achieve the twin objectives outlined above. Origami is an ancient Japanese art of producing intricate models through folding a piece of paper or card with only two types of folding creases, namely, the valley and the mountain creases. A folding pattern is produced by combining and arranging those creases. In the past, various origami patterns were applied in the design of thin-walled deployable cylinders in aerospace engineering for the purpose of compact packaging [22–25]. In the origami crash box concept, the pattern acts as a type of geometric imperfection both to reduce peak force and to activate a collapse mode that is efficient in terms of energy absorption.

This is the first of the two papers with respect to the origami crash box. It deals with the geometric design and numerical simulation of the novel box whereas the subsequent paper is on experiments. The layout of this article is as follows. First, the geometric design of the novel origami crash box is outlined and discussed in Sec. 2. Subsequently, a series of origami crash boxes with varying geometry are designed in Sec. 3. The finite element modeling approach applied to simulate the axial crushing of the origami crash box is also presented in this section. The numerical simulation results are presented and discussed in Sec. 4. The conclusions are found in Sec. 5.

2 Design of the Origami Crash Box

2.1 Geometry. The origami crash box uses the origami pattern shown in Fig. 1(*a*). The solid lines in the figure stand for hill creases and the dashed ones for valley creases. Gradually folding a flat sheet along the creases and then joining the two opposite free edges, a square origami crash box shown in Fig. 1(*b*) can be

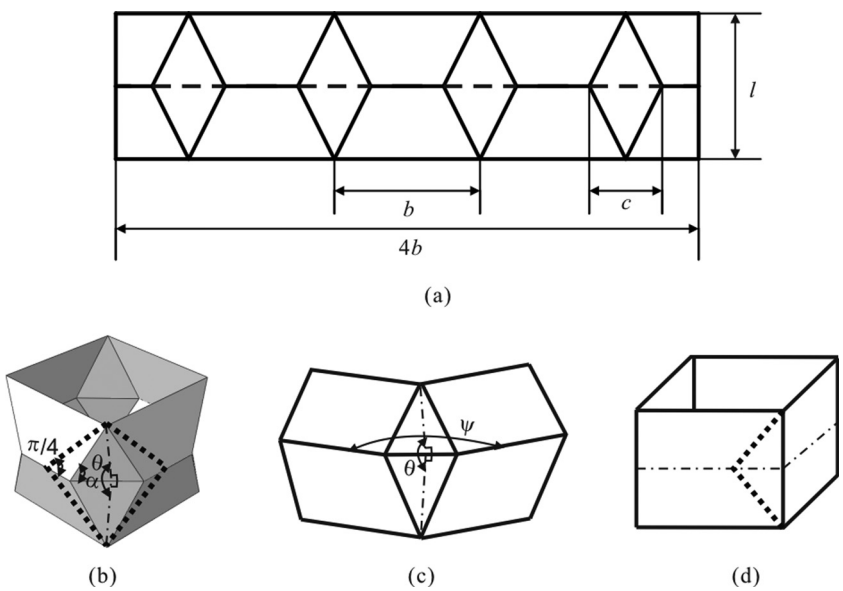

Fig. 1 (*a*) A module of the origami pattern, (*b*) a module of the origami crash box, (*c*) a quarter of the origami pattern partially folded, and (*d*) a conventional square tube

constructed; now consider, only a quarter of the pattern shown in Fig. 1(*a*), whose partially folded configuration is shown in Fig. 1(*c*). There is a one to one relationship between the dihedral angle, θ, and the corner angle, ψ,

$$\psi = \pi - 4\arctan\left(\frac{l}{c}\cos\frac{\theta}{2}\right) \tag{4}$$

When the sheet is completely flat, both θ and ψ are equal to π. When ψ reaches $\pi/2$, the folded quarter of the pattern forms a corner of a tube. Four such corners complete a square origami crash box shown in Fig. 1(*b*) due to symmetry. Equation (4) then reduces to

$$\theta = 2\arccos\left[(\sqrt{2}-1)\frac{c}{l}\right] \tag{5}$$

which gives the dihedral angle when the origami crash box is formed.

This proves the origami crash box can be formed from a flat sheet. In other words, The surface is developable.

The most important geometric feature of the origami crash box that distinguishes it from a conventional square tube shown in Fig. 1(*d*) is the lobe at each corner.

Three independent geometric parameters define the origami pattern in Fig. 1(*a*): tube width b, corner width c, and module length l. In addition, geometric constraints on c require that:

- $c \le b$, as otherwise the adjacent lobes at the corners would intercept with each other
- $c \le (\sqrt{2}+1)l$, since $\cos(\theta/2) \le 1$

When $c = 0$, the origami crash box reduces to a conventional square tube.

The pattern has several desirable properties. First, what is presented in Fig. 1(*a*) can be taken as a module, and longer tubes can be obtained by stacking a number of modules axially. Second, the pattern can be easily modified to make origami crash boxes of rectangular, polygonal cross sections or tapered shapes. This is a very useful feature as those tube profiles are frequently employed for practical energy absorption devices.

2.2 Theoretical Foundation. The load bearing capacity of a structure depends critically on structural profiles. For instance, a "T" section will exhibit different bending stiffness from that of an "I" section, provided that they have identical cross section area. Structural engineers have been able to design very efficient structural members to suit various loading scenarios by exploiting this principle. The main difficulty in applying this principle to the design of thin-walled energy absorption devices, however, lies in that the energy absorption occurs at the postbuckling stage which is highly nonlinear and thus, cannot be effectively manipulated by conventional structural design approaches.

To overcome this difficulty, the approach adopted in this paper is to prefold a thin-walled tube using the origami pattern so that the buckling and postbuckling behavior of the tube can be controlled and adjusted. The rationale behind this approach is that, if a tube has a prefolded pattern on it, the structure may follow this pattern during a crash. Hence, the collapse mode is determined by the pattern put on. Alternation of the pattern can then change the collapse mode, and high energy absorption can be achieved provided that a correct mode is chosen and this mode is followed during crushing.

When a conventional square tube crashes subjected to a compressive load, it is known from Sec. 1 that three main deformation mechanisms exist, i.e., stationary plastic hinge line in both the symmetric and extensional modes, traveling plastic hinge line in the symmetric mode, and circumferential extension in the extensional mode. Circumferential extension is very efficient in terms of energy absorption but hard to be activated in thin-walled tubes because a thin sheet is more easily bent than stretched. Traveling plastic hinge line is another type of deformation mechanism, responsible for two-thirds of the total energy absorption of a square tube collapsing in the symmetric mode. On a conventional tube, one pair of traveling hinge lines forms at each corner, which is shown in dotted lines in Fig. 1(*d*). To increase the number of traveling hinge lines, the origami crash box has two pairs of inclined prefolded creases at each corner. It is hoped that these crease lines would become traveling hinge lines during a crash and therefore, the overall energy absorption capability is increased.

Why the designed creases will become traveling hinge lines lies on the geometric compatibility when the origami crash box is crashed. Imagine that the origami crash box is made from a card and the inclined creases forming the lobe have an inclination angle α as shown in Fig. 1(*b*). α has to reduce considerably when the box folds up, i.e., the height of the box reduces. For instance, if α is $\pi/3$ initially, it will reach $\pi/4$ once the height of the box becomes zero. The change in α indicates that the inclined creases have to travel, resulting in traveling hinge lines. Moreover, the smaller α is, the lower the peak force. When a suitable α is selected, it is possible to achieve the twin conditions for a good crash box design. Next, we shall explain how this is achieved through extensive analysis.

3 Numerical Simulation

3.1 Numerical Models. A total of twenty-four origami crash boxes with various geometries were analyzed to investigate the collapse mode and energy absorption properties of the origami crash box. A conventional square tube was used as a benchmark. The width, height, and wall thickness of the conventional square tube, A0, were $b = 60$ mm, $H = 120$ mm, and $t = 1.0$ mm. A geometric imperfection in the form of a small dent was introduced near the upper end of the tube in order to ensure a stable and progressive collapse mode. All of the origami crash boxes had identical width and surface area to those of A0. Parameters c, l, and t, on the other hand, were systematically varied to investigate the influences of nondimensional geometric parameters c/l, l/b, and b/t on tubes performance. The configurations of all of the tubes are listed in Tables 1 and 2, in which M denotes the number of modules in the axial direction of the tubes. The peak force, $P_{\max}$, and mean crushing force, P_m, of each tube were generated from the results of numerical simulation. Note that P_m was calculated using,

$$P_m = \frac{\int_0^{\delta} P(x)dx}{\delta} \tag{6}$$

in which δ is the final crushing distance.

Commercial finite element analysis software package ABAQUS/Explicit [26] was applied to simulate the axial crushing process. The crushing scenario was modeled as a tube standing on a stationary rigid panel and being compressed by a moving one. Only half of the tube was modeled because of symmetry. The upper and lower ends of the tube were coupled to the moving and stationary rigid panels, respectively, by three translational degrees of freedom. Symmetric boundary conditions were assigned to the tube edges on the plane of symmetry. The stationary rigid panel was completely fixed, whereas all of the degrees of freedom of the moving rigid panel were constrained except for the translational one in the axial direction of the tube. Prescribed downward displacement was assigned to the free degree of freedom of the moving rigid panel to control the crushing process, and smooth amplitude definition built in ABAQUS was assigned to the control the loading rate. The final crushing distance was so chosen that the residual height was 35 mm for all of the tubes. Four-node shell elements with reduced integration S4R were used to mesh the tube, supplemented by a few triangular elements to avoid excessively small or distorted elements. Self-contact was employed to

Table 1 Tube geometries and numerical results

Model	c (mm)	l (mm)	θ (deg)	M	t (mm)	P_{max} (kN)	P_{max} reduction	P_m (kN)	P_m increase	Collapse mode
A0	—	—		—	1.0	40.17	—	11.98	—	—
A1_1	20	40	156	3	1.0	25.00	37.8%	19.03	58.9%	CDM
A1_2	16	40	160	3	1.0	25.74	35.9%	18.73	56.3%	CDM
A1_3	13.3	40	164	3	1.0	24.41	39.2%	19.35	61.5%	CDM
A1_4	10	40	168	3	1.0	25.35	36.9%	20.12	68.0%	CDM
A1_5	6.7	40	172	3	1.0	25.37	36.8%	18.77	56.7%	IDM
A2_1	15	30	156	4	1.0	24.54	38.9%	19.49	62.7%	CDM
A2_2	12	30	160	4	1.0	27.80	30.8%	20.93	74.7%	CDM
A2_3	10	30	164	4	1.0	25.02	37.7%	21.15	76.5%	CDM
A2_4	7.5	30	168	4	1.0	24.51	39.0%	20.95	74.9%	IDM
A2_5	5	30	172	4	1.0	26.20	34.8%	19.16	59.9%	IDM
A3_1	12	24	156	5	1.0	26.46	34.1%	21.66	80.8%	CDM
A3_2	9.6	24	160	5	1.0	25.14	37.4%	22.25	85.7%	CDM
A3_3	8	24	164	5	1.0	25.39	36.8%	22.27	85.9%	CDM
A3_4	6	24	168	5	1.0	24.71	38.5%	20.28	69.3%	IDM
A4_1	10	20	156	6	1.0	31.77	20.9%	23.01	92.1%	CDM
A4_2	8	20	160	6	1.0	23.69	41.0%	21.34	78.1%	IDM
A5_1	8.6	17.2	156	7	1.0	27.19	32.3%	20.26	69.1%	IDM

Table 2 Tube geometries with various thickness and numerical results

Model	c (mm)	l (mm)	θ (deg)	M	t (mm)	P_{max} (kN)	P_m (kN)	Collapse mode
A6_1	20	40	156	3	0.6	10.76	7.86	CDM
A6_2	20	40	156	3	0.8	16.56	12.95	CDM
A6_3	20	40	156	3	1.2	33.93	26.09	CDM
A6_4	20	40	156	3	1.4	46.28	34.33	CDM
A6_5	20	40	156	3	1.6	51.42	44.98	CDM
A6_6	20	40	156	3	1.8	62.27	56.11	CDM
A6_7	20	40	156	3	2.0	83.26	65.60	CDM

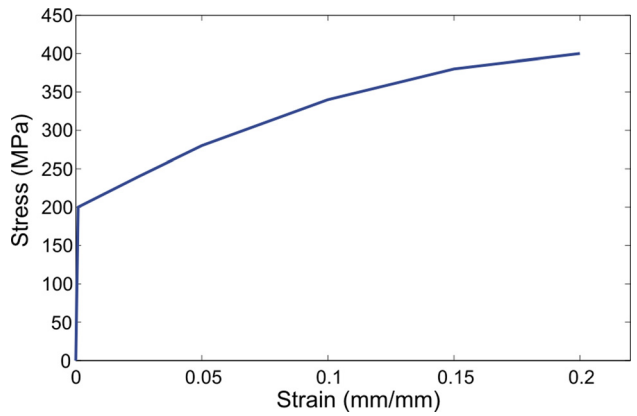

Fig. 2 Material engineering stress–strain curve

model the contacts among different parts of the tube, and surface-to-surface contact was defined between the tube and each rigid panel. Friction was also considered and the friction coefficient μ was taken as 0.25 [26].

Mild steel, commonly used for tubular energy absorption devices, was chosen as the material. The mechanical properties are: density $\rho = 7800$ Kg/m^3, Young's Modulus $E = 210$ GPa, $\sigma_y = 200$ MPa, $\sigma_u = 400$ MPa, ultimate strain $\varepsilon_u = 20.0\%$, Poisson's ratio $\nu = 0.3$, and $n = 0.34$. The engineering stress versus strain curve is plotted in Fig. 2 [26].

Convergence tests with respect to mesh density and analysis time, respectively, were also conducted prior to the analysis. Two principles recommended by ABAQUS [27] were checked:

- The ratio of artificial energy to internal energy is below 5% to make sure that hour-glassing effect would not significantly affect the results.
- The ratio of kinetic energy to internal energy is below 5% during most of the crushing process to ensure that dynamic effect can be considered as insignificant.

It was found out that a global mesh size of 1 mm and an analysis time of 0.02 s yielded satisfactory results.

3.2 Validation of Numerical Models. The numerical models of the conventional square tube and the origami crash box were validated against the experimental results [28] of a number of physical samples. For example, one set of samples had $b = 60$ mm, $H = 120$ mm, and $t = 0.5$ mm for the conventional tube, and $b = 60$ mm, $c = 30$ mm, $l = 60$ mm, $M = 2$, and $t = 0.5$ mm for the origami crash box. The material in hand at the time for physical models had the following properties: $E = 220.8$ GPa, $\sigma_y = 245.6$ MPa, $\sigma_u = 369.2$ MPa, and $\varepsilon_u = 25.0\%$. It was found that in the case of the conventional tube, the symmetric mode appeared in both simulation and experiment. The mean crushing forces, 4.75 kN for the numerical model and 4.78 kN for the physical sample, matched quite well. Moreover, the numerical model of the origami crash box also showed identical collapse mode to those of the physical samples. And a reasonable match between the mean crushing force of the numerical model, 5.42 kN, and those for the physical ones, 5.50 kN and 5.84 kN, was achieved.

4 Results

4.1 Axial Crushing of Conventional Square Tube. The conventional square tube A0 was analyzed to set a benchmark to evaluate the energy absorption enhancement of the origami crash box. The axial crushing process of A0 is shown in Fig. 3(*a*). Note that only a quarter of the tube is presented in order to highlight the deformation in the critical corner areas. A0 collapses from the upper end where the dent is placed, is then progressively folded three times axially through the initiation and propagation of horizontal stationary and inclined traveling plastic hinge lines, and eventually forms the symmetric mode. The corresponding equivalent plastic strain (PEEQ) contour maps of A0, which are plotted on the undeformed shape for clarity, are shown in Fig. 3(*b*). It can be seen that large plastic strain concentrates on the stationary plastic hinge lines and the corner areas where the traveling plastic

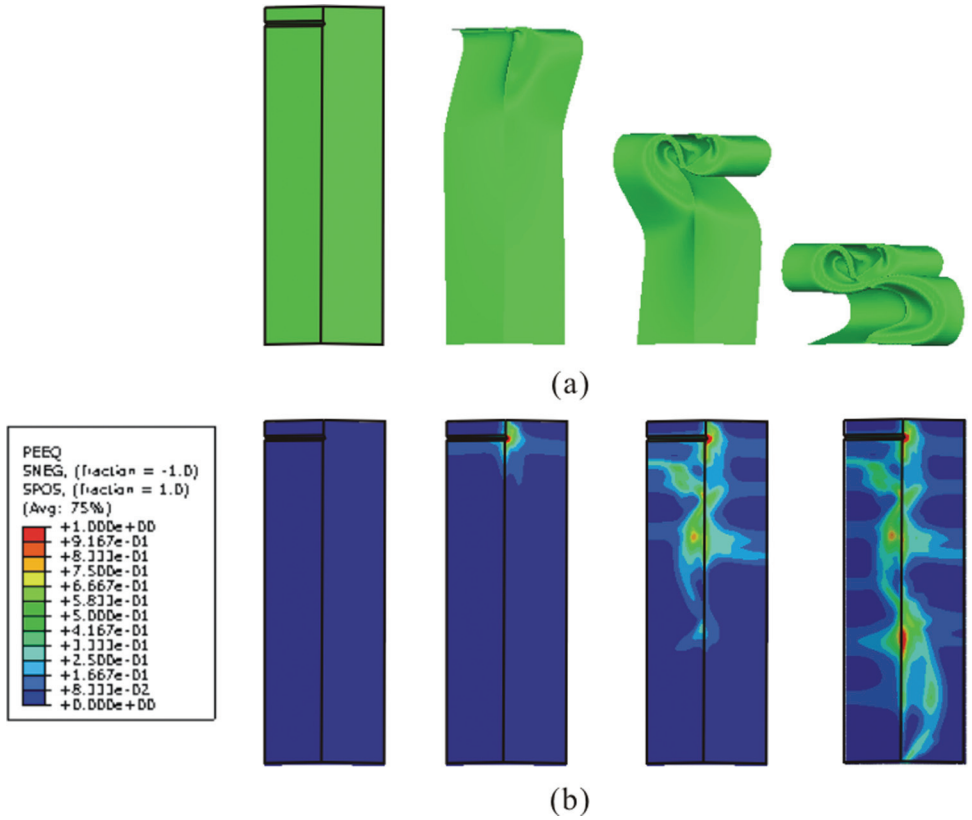

Fig. 3 (*a*) Crushing process of A0, and (*b*) PEEQ contour maps of A0

hinge lines are located, whereas the remaining panels undergo negligible plastic deformation.

The force versus displacement curve of A0 is plotted in Fig. 4. The curve starts with a very high $P_{\max}$ of 40.17 kN, followed by a number of crests and troughs. The numerical value of P_m, 11.98 kN as listed in Table 1, agrees reasonably well with the theoretical value of 12.49 kN, calculated using Eq. (1), indicating that the finite element modeling procedure is appropriate for the problem analyzed here. The numerical value being slightly lower than the theoretical value is attributed to the fact that essentially pinned boundary conditions at the two ends of the tube were applied in the numerical analysis, whereas clamped boundary conditions were assumed in the derivation of Eq. (1) [11,12]. Applying clamped boundary conditions to A0, the numerical value of the mean crushing force was 12.50 kN, which coincided with the theoretical value 12.49 kN.

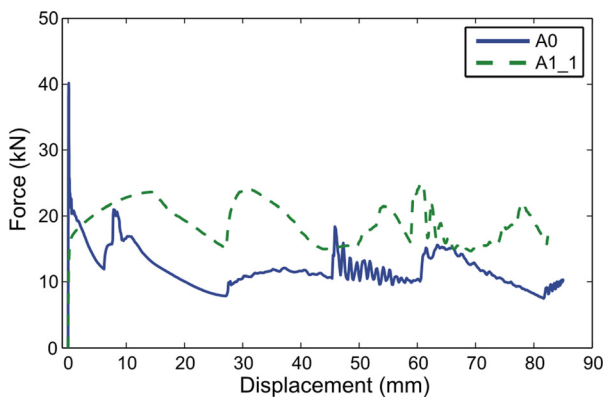

Fig. 4 Force versus displacement curves of A0 and A1_1

4.2 Axial Crushing of Origami Crash Box. Tube A1_1, which has three modules, is chosen here as the representative of the origami crash boxes. The three modules of the tube are referred to as modules I–III from top to bottom. Figure 5(*a*) shows the crushing process of a quarter of A1_1, and the corresponding contour maps on undeformed shape are plotted in Fig. 5(*b*). It can be seen that A1_1 collapses following the premanufactured origami pattern on the surface in a progressive and stable manner. At the beginning, module II first starts to fold. The second configuration in Fig. 5(*a*) indicates that two pairs of traveling plastic hinge lines are formed along the four sides of the lobe in the module. This observation is also reflected in the second PEEQ contour map in Fig. 5(*b*), which shows that large plastic deformation occurs along the four sides. As the tube is further compressed, the traveling plastic hinge lines move away from each other, deforming the corner areas, as can be observed from the third configuration in Fig. 5(*a*). The third PEEQ contour map in Fig. 5(*b*) shows that large plastic strain takes place in the corner areas, too. Meanwhile, horizontal stationary plastic hinge lines are formed near the upper and lower ends of the module, respectively. Those hinges are not exactly along the ends of the module but at locations inside the module, which can be seen from the third configurations in Fig. 5(*a*) and the third PEEQ contour map in Fig. 5(*b*). As a result, the module is not completely flattened but has a residual height. The horizontal stationary plastic hinge line in the middle of the module, initiated at the beginning of the crushing process, is also completely folded at this point. Subsequently modules I and III are folded one after another in a similar manner until the tube is completely crushed. Another observation that can be made from the PEEQ contour maps in Fig. 5(*b*) is that large plastic deformation is limited to the areas swept by the traveling plastic hinge lines and the neighborhood of the stationary plastic hinge lines, whereas the remaining panels undergo small plastic deformation. This observation indicates that no circumferential membrane deformation of a large magnitude occurs, further supporting

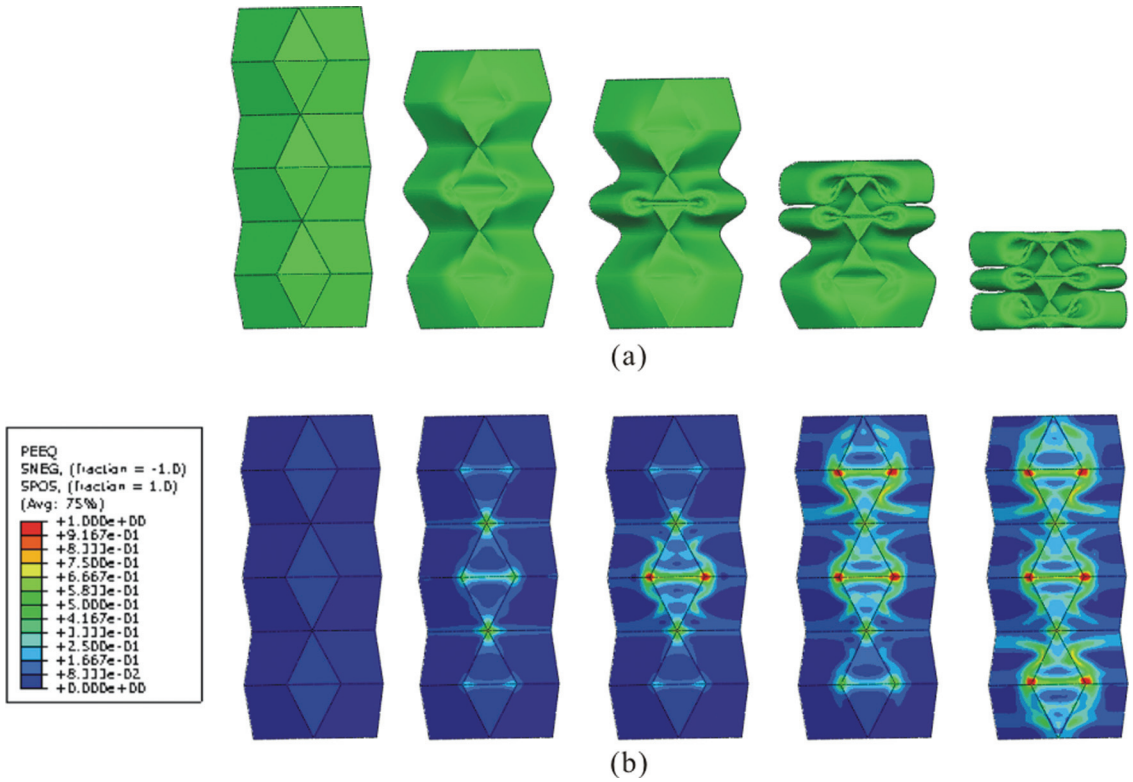

Fig. 5 (*a*) Crushing process of A1_1, and (*b*) PEEQ contour maps of A1_1

that traveling plastic hinge lines are activated in the tube. Comparing this collapse mode with the diamond mode of circular tubes reveals that the two modes are quite similar in shape, except that the origami crash box is composed of flat plates instead of curved shells. Therefore, the collapse mode of A1_1 is referred to as the complete diamond mode (CDM), in which all of the lobes develop well during the crushing process.

The force versus displacement curve of A1_1 is also plotted in Fig. 4. It can be seen that high peak force no longer exists at the beginning of the crash, leading to a considerably lower $P_{\max}$ of A1_1 than that of A0. On the other hand, the area below the curve of A1_1, which indicates the energy absorption capacity, is substantially larger than that of A0. The numerical data in Table 1 show that $P_{\max}$ of A1_1 is 25.00 kN, 37.8% lower than that of A0, whereas P_m of A1_1 is 19.03 kN, 58.9% higher than that of A0. Therefore, it can be concluded that the origami pattern has successfully created a thin-walled tube with low peak force and high mean crushing force.

4.3 Effects of Ratios *c*/*l* and *l*/*b*. It has been shown that the complete diamond mode is more efficient in terms of energy absorption than the symmetric mode. Therefore, a key task in the design of the origami crash box is to determine the range of pattern geometry that is able to trigger the complete diamond mode and the optimum pattern geometry that leads to maximum energy absorption.

Ratio c/l, which increases with decreasing θ following Eq. (4), is a crucial factor to determine whether the complete diamond mode occurs and how traveling plastic hinge lines propagate if it does occur. It is not difficult to infer that the pattern would no longer be followed if c/l is too small, leading to low energy absorption. On the other hand, a very large c/l, while ensuring the following of the pattern, is also undesirable from the perspective of energy absorption as it would reduce the areas swept by traveling plastic hinge lines. In addition, the amount of rotation of stationary plastic hinge lines is also reduced.

Ratio l/b, which is inversely proportional to M for an origami crash box with fixed width and surface area, is another important factor that influences the performance of the origami crash box. It is intuitive that the smaller the ratio l/b, or the more the modules in a tube, the higher the energy absorption. This is because more modules lead to more horizontal stationary plastic hinge lines. However, a very small l/b would not only make the tube geometry complicated but could also result in the pattern being overridden during the crushing process.

Sixteen more origami crash boxes, A1_2–A5_1, which had width and surface area identical to those of A0, were also analyzed to investigate the effects of c/l and l/b. The results are organized based on variations of θ and M in Table 1.

The collapse modes of the tubes are first looked into. The crushed configurations of A1_2–A1_5, all of which have $M = 3$, are presented in Figs. 6(*a*)–6(*d*). When $\theta \leq 168$ deg (A1_2, A1_3, and A1_4), the pattern is well followed and the complete diamond mode is successfully attained. When θ reaches 172 deg, however, it can be seen from the crushed configuration of A1_5 in Fig. 6(*d*) that although the pattern is still followed, traveling plastic hinge lines fail to be activated in the middle module of the tube, resulting in that the lobes in that module do not develop well. If M reaches 4, like in the case of $M = 3$, the collapse mode still transits from the complete diamond mode seen in A2_1 with $\theta = 156$ deg, Fig. 6(*e*), to the mode featuring under folded lobes seen in A2_4 with $\theta = 168$ deg, Fig. 6(*f*). But unlike in the case of $M = 3$, it is observed from A2_5 with $\theta = 172$ deg, Fig. 6(*g*), that the pattern is no longer followed and the two modules at the lower half of the tube merge. As a result, A2_5 are axially folded only three times instead of four as the design intended. Similar phenomena can also be observed in A3_4 in Fig. 6(*h*), and A4_2 in Fig. 6(*i*). When $M = 7$, A5_1 in Fig. 6(*j*), the pattern is not followed when $\theta = 156$ deg. No further reduction in θ was attempted as the results have been sufficiently clear to draw conclusions upon.

Two conclusions can be drawn from the results presented above:

- For tubes with identical M, the complete diamond mode is usually triggered when θ is relatively small, and then ceases

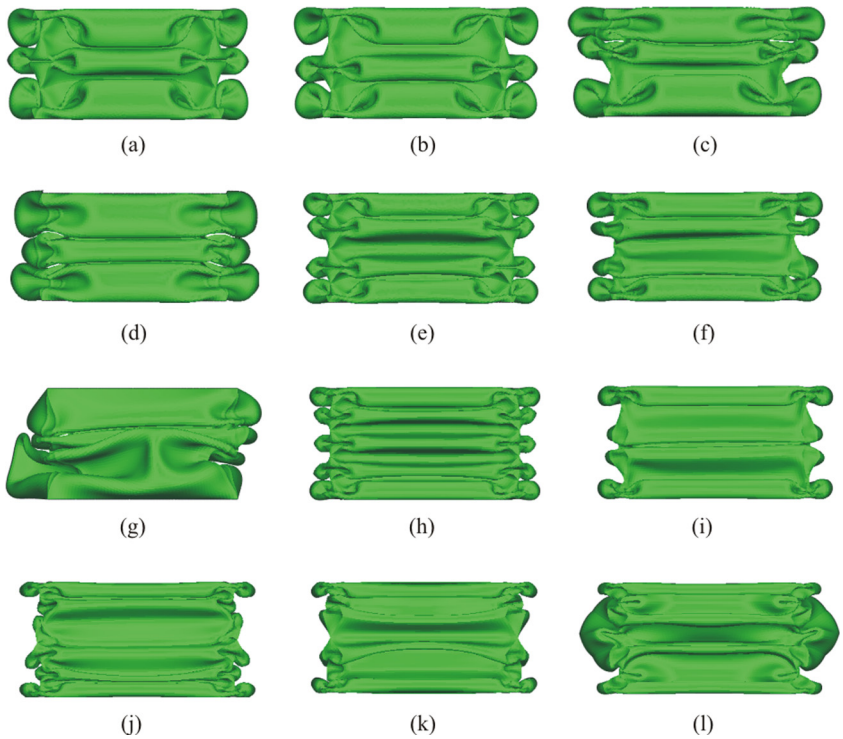

Fig. 6 Crushed configurations of (*a*) A1_2, (*b*) A1_3, (*c*) A1_4, (*d*) A1_5, (*e*) A2_1, (*f*) A2_4, (*g*) A2_5, (*h*) A3_1, (*i*) A3_4, (*j*) A4_1, (*k*) A4_2, and (*l*) A5_1

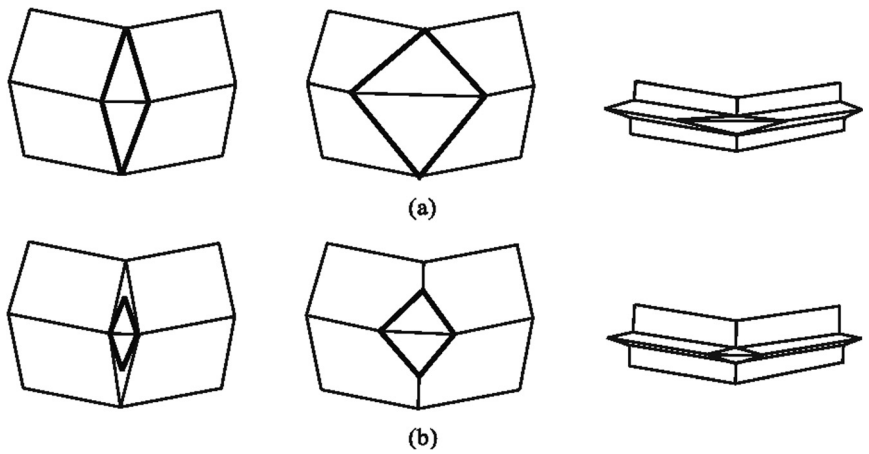

Fig. 7 Schematic diagrams of (*a*) the complete diamond mode, and (*b*) the incomplete diamond mode

to appear as θ surpasses a critical value where collapse modes featuring either under development of the lobes or the pattern not being followed occur, see A1_5, A2_4, A2_5, A3_4, A4_2, and A5_1. Note that there are no rigorous criteria to determine whether the lobes develop "well" or not, and thus, this is done based mainly on visual inspection. Those collapse modes are named the incomplete diamond mode (IDM) here, as opposed to the complete diamond mode shown in A1_1, A2_1, and A3_1. A schematic diagram of the crushing process of a quarter of a module of the origami crash box is drawn in Fig. 7 in order to highlight the difference between the complete and the incomplete diamond modes. For the complete diamond mode shown in Fig. 7(*a*), the prefolded inclined creases highlighted by bold lines at the corner will form traveling plastic hinge lines that subsequently travel. On the other hand, in the incomplete diamond mode shown in Fig. 7(*b*), the prefolded creases do not transform to traveling plastic hinge lines. Instead, new and shorter inclined plastic hinge lines, also highlighted by bold lines, form and travel in the subsequent crushing process. The positions and lengths of these traveling plastic hinge lines account for the difference of the two collapse modes.

- When 156 deg $\leq \theta \leq$ 172 deg, the pattern is always followed for $M = 3$. If $M > 3$, θ gets smaller as M increases in order for the prefolded pattern to be followed. Recalling that the conventional tube A0 forms three folds axially, we speculate that if M is identical to the number of folds in the corresponding conventional tube, the complete diamond mode is the most stable. This conjecture can be explained from the perspective of energy. When a geometrically perfect square tube collapses, the number of folds naturally formed, which is three in this case, corresponds to the lowest energy, or the most stable mode. The function of the origami pattern is to distract the tube from its natural

collapse mode via prefolding at each corner with inclined creases to increase the number of traveling plastic hinge lines in each fold and via setting the number of modules to increase the number of folds axially. Hence, the closer the new collapse mode of the origami crash box is to the natural mode of the corresponding conventional tube, the more stable the new collapse mode becomes. A greater M would further deviate the collapse mode of the origami crash box from the natural one, making it harder for the pattern to be followed. Wu investigated the influence of number of modules for another family of tubes with prefolds numerically [29]. The same could be applied to the origami crash box. However, the underlying principle in determining M for the formation of the complete diamond mode still warrants further investigation.

Subsequently, the energy absorption properties of the tubes are investigated. The numerical data of the tubes are summarized in Table 1. In addition, P_m versus θ and M are plotted in Figs. 8(*a*) and 8(*b*), respectively, and $P_{\max}$ versus θ and M, are plotted in Figs. 8(*c*) and 8(*d*), respectively. Both P_m and $P_{\max}$ have been normalized against those of the conventional one. Four observations can be made from those results.

First of all, Fig. 8(*a*) shows that for tubes with identical M, P_m tends to increase with θ, provided that the complete diamond mode is successfully triggered, but the increment is minor. For instance, at $M = 4$, P_m first slightly rises from $\theta = 156$ deg to $\theta = 164$ deg within which the complete diamond mode is always obtained. Similar trends can also be observed at $M = 3$ and 5. The only exception is A1_2 with $\theta = 156$ deg has a lower P_m than that of A1_1 with $\theta = 160$ deg, both of which collapse in the complete diamond

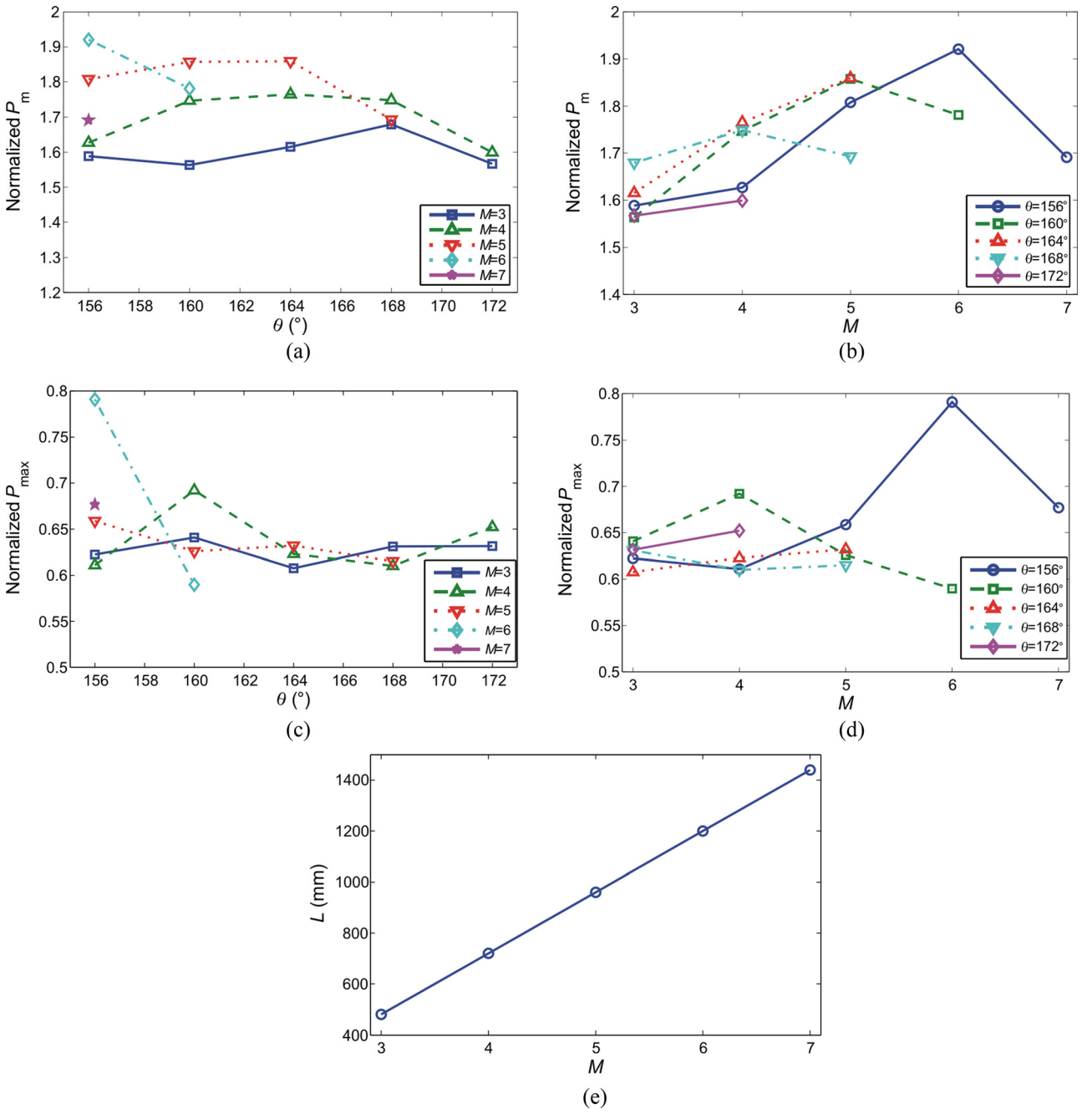

Fig. 8 (*a*) Normalized mean crushing force versus dihedral angle curves, (*b*) normalized mean crushing force versus number of modules curves, (*c*) normalized peak force versus dihedral angle curves, (*d*) normalized peak force versus number of modules curves, and (*e*) length of stationary plastic hinge lines versus number of modules curves of A1_1–A5_1

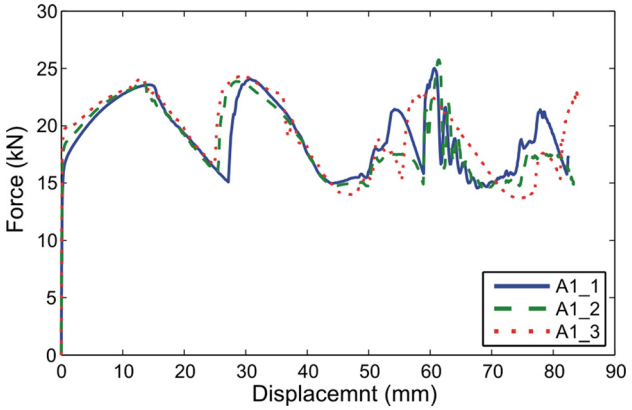

Fig. 9 Force versus displacement curves of A1_1, A1_2 and A1_3

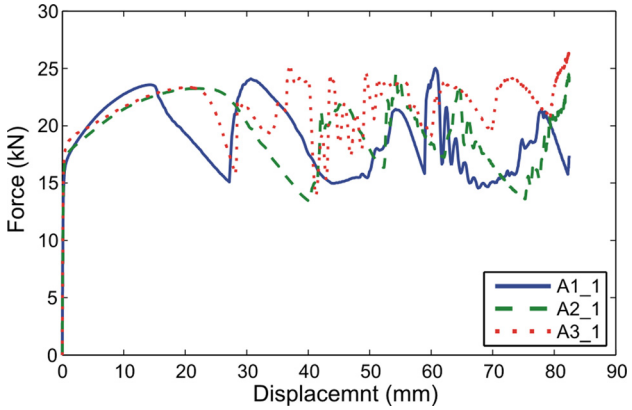

Fig. 10 Force versus displacement curves of A1_1, A2_1 and A3_1

mode. The explanation is as follows. On one hand, θ determines the corner areas swept by traveling plastic hinge lines and the rotation angles of stationary plastic hinge lines. The larger θ, the larger the corner areas and the rotation angles, leading to a slight increase in P_m. On the other hand, the energy absorption of a tube is primarily determined by the collapse mode it takes. Therefore, as long as the collapse mode is identical, the energy absorption is close. The force versus displacement curves of A1_1, A1_2, and A1_3, which have identical M and increasing θ, are plotted in Fig. 9. It can be seen that the three curves are all quite similar in shape, and the curve of A1_3 are generally slightly higher than that of A1_2 which is higher than that of A1_1.

Secondly, it can be seen from Figs. 8(*c*) and 8(*d*) that $P_{\max}$, in contrast to P_m, shows no obvious close correlation to θ or M for the ranges that are considered in this analysis. This phenomenon is also understandable because after the elimination of the very high initial buckling force, the location and magnitude of $P_{\max}$ show certain degree of randomness. Again, the variation in $P_{\max}$ is not substantial.

Thirdly, the switch from the complete diamond mode to the incomplete diamond mode, such as from A1_4 to A1_5, from A2_3 to A2_4, and from A3_3 to A3_4, is usually accompanied by a drop in P_m. This observation again confirms that the new collapse mode mainly accounts for the increase in energy absorption. If the collapse mode of a tube deviates from the complete diamond mode, the energy absorption also reduces.

Finally, as shown in Fig. 8(*b*), for tubes with identical θ, P_m increases with M provided that the complete diamond mode is obtained. However, the increment is not large, and P_m of most tubes fall into the range of 20 ± 2 kN, indicating that increasing M would not substantially improve the energy absorption of the origami crash box. The force versus displacement curves of A1_1, A2_1, and A3_1, which have identical θ but increasing M, are plotted in Fig. 10, as an example. It can be seen that although the curve shapes in terms of the number of crests and troughs are different from each other, the areas below the curves, which represent the energy absorption of the tubes, are 1568.1, 1606.0, and 1784.8 J, respectively, with a variation of 13.8% when M is increased from 3 to 5. A qualitative explanation to this observation involves different energy dissipation mechanisms in the collapse process. Two of the main sources of energy dissipation are the rotation of stationary plastic hinge lines and the sweeping of traveling plastic hinge lines; although the total length of stationary plastic hinge lines, L, increases with M, as shown in Fig. 8(*e*), the corner areas swept by traveling plastic hinge lines shrink since the height of each module is reduced, as clearly observed by comparing A1_1, A2_1, and A3_1 shown in Figs. 5, 6(*e*) and 6(*h*), respectively. The energy absorption enhancement contributed by extra stationary plastic hinge lines is comparable to the energy absorption reduction due to the shrunk corner areas swept by traveling plastic hinge lines, resulting in only minor net energy absorption difference.

4.4 Effects of Ratio *b*/*t*. As mentioned in Sec. 1, ratio b/t is an important factor that influences the collapse mode of a thin-walled square tube. Different collapse modes can be triggered when b/t varies, resulting in very different energy absorption capabilities.

Seven origami crash boxes, A6_1–A6_7, are analyzed to investigate the effects of b/t. All of the tubes have identical geometry with that of A1_1 except that t varies from 0.6 mm to 2.0 mm; thus covering the range of $30 \leq b/t \leq 100$. It is shown from the results in Table 2 that the crushing process of the tube is not noticeably affected by b/t and the complete diamond mode is consistently obtained. Data collected from automakers such as Range Rover, MG Rover, and BMW indicate that commercial crash boxes usually have b/t of 30–60. Therefore, the collapse mode of the origami crash box can be seen as independent of b/t, which is a desirable characteristics in the design of crash boxes.

5 Discussion

5.1 Half Tube Model Versus Full Tube Model. The half tube model, rather than a full tube model, was used in the numerical simulation for the following reasons. First, all the tubes are relatively short with tube height to cross section width ratio around 2, which are expected to buckle progressively [30]. Reduced models were often used in the past to simulate axial crushing of such short tubes [20,31]. Second, the half tube model can also model some global buckling modes of collapse since it is constrained only in one plane of symmetry. Third, the half tube model is less sensitive to small numerical errors than full 3D tube model, which could lead to fictitious collapse modes [32]. In addition, one of the tubes (A1_1) was analyzed using both the full tube model and the half tube model, respectively. It was found that the collapse modes obtained from both models were symmetric and progressive. Their mean crushing forces, 18.94 kN for the full tube model and 19.03 kN for the half tube model, also matched very well. Therefore, the half tube model was used for all of the other tubes.

5.2 Quasi-Static Analysis Versus Dynamic Analysis. The crash boxes are always subjected to dynamic loading in a real world collision. The impact speed adopted in the design of crash boxes is usually within the range of low to medium velocity of under 20 m/s. Although quasi-static analysis has been used in this paper, dynamic analysis has also shown a similar trend. To demonstrate the performance of the origami crash box subjected to dynamic loading, the crushed configurations of model A1_1 under dynamic loading of 20 m/s constant velocity is shown in Fig. 11(*a*), as an example. The Cowper–Symonds relation [29] was employed in the dynamic analysis to take material strain rate effect into consideration. It can

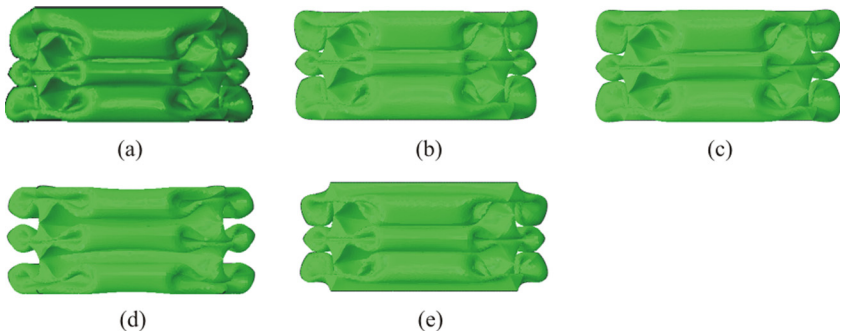

Fig. 11 Crushed configurations of A1_1 (*a*) subjected to dynamic loading, (*b*) assigned to high strength steel, (*c*) assigned to aluminum alloy, (*d*) subjected to free-free boundary conditions, and (*e*) subjected to fixed-fixed boundary conditions

be seen that the new complete diamond mode is still retained under the dynamic loading, indicating that the novel origami crash box is suitable for impact applications.

5.3 Effects of Material Properties. The origami crash boxes analyzed so far are made from mild steel, a material commonly used for crash boxes. However, the concept is purely structural and not associated with a particular material. It is expected that crash boxes made from other ductile materials would also exhibit similarly favorable crash performance. To confirm that, two other commonly used ductile materials, the high strength steel and aluminum alloy, were, respectively, assigned to model A1_1 and the axial crushing analysis was conducted. The properties of the materials are $\rho = 7800$ Kg/m^3, $E = 210$ GPa, $\nu = 0.3$, $\sigma_y = 406$ MPa, $\sigma_u = 819.6$ MPa, and $\varepsilon_u = 17.6\%$ for the high strength steel and $\rho = 2700$ Kg/m^3, $E = 68.2$ GPa, $\nu = 0.3$, $\sigma_y = 80$ MPa, $\sigma_u = 173$ MPa, and $\varepsilon_u = 17.3\%$ for aluminum alloy. The crushed configurations of A1_1 associated with the two materials are presented in Figs. 11(*b*) and 11(*c*), respectively. It can be seen that the complete diamond mode is successfully triggered in both cases. These results indicate that the complete diamond mode is insensitive to material properties; thus demonstrating the robustness of the performance of the origami crash box.

Obviously, brittle materials would be unsuitable for the origami crash box since the collapse of the origami crash box involves large plastic deformation.

5.4 Effects of Boundary Conditions. Pinned-pinned boundary conditions have been considered in this paper. This is because commercial crash boxes are commonly installed in a car through spot-welding one end to a mounting plate and bolting the other to a bumper beam, which are close to pinned-pinned boundary conditions. However, in practice crash boxes could be subjected to various other boundary conditions depending on the installation methods. For those crash boxes whose ends are connected to a mounting plate and a bumper beam, respectively, through seam welding, the fixed-fixed boundary conditions are more appropriate.

We analyzed model A1_1 under both free-free and fixed-fixed boundary conditions, respectively. The collapse modes are shown in Figs. 11(*d*) and 11(*e*). It can be seen that the complete diamond mode has invariably been triggered irrespective of boundary conditions. The complete diamond mode is therefore insensitive to boundary conditions. Moreover, the mean crushing forces of A1_1 under both types of boundary conditions are very close to that under pined-pinned boundary conditions. The same conclusion can also be obtained for peak forces.

5.5 Summary. A novel origami pattern has been proposed to design a type of high-performance energy absorption device called the origami crash box. Numerical simulation results show that a new and more efficient collapse mode in terms of energy absorption, namely the complete diamond mode which features increased traveling plastic hinge lines, can be successfully triggered in the origami crash box within a wide range of pattern geometry. As a result, both peak force reduction of more than 30% and mean crushing force increase of over 50% are obtained for the origami crash box in comparison with those of conventional square tubes with identical weight.

A parametric study has also been conducted to investigate the effects of geometric parameters, including the dihedral angle θ, the number of modules M, and the tube width to wall thickness ratio b/t, on the collapse mode, peak reaction force $P_{\max}$, and mean crushing force P_m of the origami crash box. The main conclusions drawn from the study are as follows.

- The critical value of θ, that is just able to trigger the complete diamond mode depends on M, and this value decreases with M. In other words, a larger amount of prefolding is needed to induce the complete diamond mode as more modules are put on a tube.
- When the complete diamond mode is triggered, increasing θ leads to increase in P_m provided that M remains the same, while increasing M results in increase in P_m provided that θ is unchanged. Therefore, generally less prefolding and more modules help to improve the energy absorption of an origami crash box.
- In the optimum case (tube model A4_1 in Table 1), as much as a 92.1% increase in P_m is achieved, while a $P_{\max}$ reduction of 20.9% is obtained in the same design in comparison with a conventional square tube of same thickness and overall surface area.
- The collapse mode of the origami crash box is independent of b/t for $30 \leq b/t \leq 100$, provided that a proper pattern geometry is selected.

A series of static and dynamic axial crushing tests have been carried out and the results will be published in a subsequent paper. Moreover, further theoretical investigation of some interesting phenomena observed in the numerical simulation, such as the critical value of θ for tubes with different configurations, is currently being conducted.

This paper is probably the first attempt to apply origami patterns to design efficient crash boxes. The successful design of the origami crash box naturally raises a question: are there other patterns that are better for applications as crash boxes? A large pool of origami patterns have been designed by origami artists [33,34], some of which could be potential candidates for crash boxes. We are currently investigating a number of other patterns and the results will be reported in due course.

Acknowledgment

J.M. would like to thank University of Oxford and Balliol College for financial support in the form of a Clarendon Scholarship

and a Jason Hu Scholarship, which has enabled him to study at Oxford. Z.Y. is also a Haitian visiting scholar at Dalian University of Technology, China. We also like to acknowledge that the work has been supported by a National Natural Science Foundation of China Overseas Collaboration Grant (11128205).

References

[1] Tyrell, D., Jacobsen, K., Martinez, E., and Perlman, A. B., 2006, "Train-to-Train Impact Test of Crash Energy Management Passenger Rail Equipment: Structural Results," ASME International Mechanical Engineering Congress and Exposition, Chicago, IL, November 5–10, ASME Paper No. IMECE2006-13597.
[2] Airoldi, A., and Janszen, G., 2005, "A Design Solution for a Crashworthy Landing Gear With a New Triggering Mechanism for the Plastic Collapse of Metallic Tubes," Aerosp. Sci. Technol., **9**(5), pp. 445–455.
[3] Lu, G., and Yu, T.X., 2003, *Energy Absorption of Structures and Materials*, CRC-Woodhead, Cambridge, UK, pp. 144.
[4] Alexander, J. M., 1960, "An Approximate Analysis of the Collapse of Thin Cylindrical Shells Under Axial Loading," Q.J. Mech. Appl. Math., **13**(1), pp. 10–15.
[5] Wierzbicki, T., Bhat, S.U., Abramowicz, W., and Brodkin, D., 1992, "Alexander Revisited—A Two Folding Elements Model of Progressive Crushing of Tubes," Int. J. Solids Struct., **29**(24), pp. 3269–3288.
[6] Singace, A.A., Elsobky, H., and Reddy, T.Y., 1995, "On the Eccentricity Factor in the Progressive Crushing of Tubes," Int. J. Solids Struct., **32**(24), pp. 3589–3602.
[7] Pugsley, A., 1960, "The Large-Scale Crumpling of Thin Cylindrical Columns," Q. J. Mech. Appl. Math., **13**(1), pp. 1–9.
[8] Pugsley, A.G., 1979, "On the Crumpling of Thin Tubular Struts," Q. J. Mech. Appl. Math., **32**(1), pp. 1–7.
[9] Singace, A.A., 1999, "Axial Crushing Analysis of Tubes Deforming in the Multi-Lobe Mode," Int. J. Mech. Sci., **41**(7), pp. 865–890.
[10] Wierzbicki, T., and Abramowicz, W., 1983, "On the Crushing Mechanics of Thin-Walled Structures," ASME J. Appl. Mech., **50**(4), pp. 727–734.
[11] Abramowicz, W., and Jones, N., 1984, "Dynamic Axial Crushing of Square Tubes," Int. J. Impact Eng., **2**(2), pp. 179–208.
[12] Abramowicz, W., and Jones, N., 1986, "Dynamic Progressive Buckling of Circular and Square Tubes," Int. J. Impact Eng., **4**(4), pp. 243–270.
[13] Santosa, S., and Wierzbicki, T., 1998, "Crash Behavior of Box Columns Filled With Aluminum Honeycomb or Foam," Comput. Struct., **68**(4), pp. 343–367.
[14] Abramowicz, W., and Jones, N., 1984a, "Dynamic Axial Crushing of Square Tubes," Int. J. Impact Eng., **2**(2), pp. 179–208.
[15] Singace, A.A., and El-Sobky, H., 1997, "Behaviour of Axially Crushed Corrugated Tubes," Int. J. Mech. Sci., **39**(3), pp. 249–268.
[16] Hosseinipour, S.J., and Daneshi, G.H., 2003, "Energy Absorbtion and Mean Crushing Load of Thin-Walled Grooved Tubes Under Axial Compression," Thin-Walled Struct., **41**(1), pp. 31–46.
[17] Lee, S., Hahn, C., Rhee, M., and Oh, J.-E., 1999, "Effect of Triggering on the Energy Absorption Capacity of Axially Compressed Aluminum Tubes," Mater. Des., **20**(1), pp. 31–40.
[18] Adachi, T., Tomiyama, A., Araki, W., and Yamaji, A., 2008, "Energy Absorption of a Thin-Walled Cylinder With Ribs Subjected to Axial Impact," Int. J. Impact Eng., **35**(2), pp. 65–79.
[19] Lee, K.S., Kim, S.K., and Yang, I.Y., 2008, "The Energy Absorption Control Characteristics of Al Thin-Walled Tube Under Quasi-Static Axial Compression," J. Mater. Process. Technol., **201**(1–3), pp. 445–449.
[20] Zhang, X., Cheng, G., You, Z., and Zhang, H., 2007, "Energy Absorption of Axially Compressed Thin-Walled Square Tubes With Patterns," Thin-Walled Struct., **45**(9), pp. 737–746.
[21] Ma, J., Le, Y., and You, Z., 2010, "Axial Crushing Tests of Thin-Walled Steel Square Tubes With Pyramid Patterns," 51st AIAA/ASME/ASCE/AHS/ASC Structures, Structural Dynamics, and Materials Conference, Orlando, FL, April 12–15, AIAA Paper No. 2010-2615.
[22] Guest, S.D., and Pellegrino, S., 1994a, "The Folding of Triangulated Cylinders—Part I: Geometric Considerations," ASME J. Appl. Mech., **61**, pp. 773–777.
[23] Guest, S.D., and Pellegrino, S., 1994b, "The Folding of Triangulated Cylinders—Part II: The Folding Process," ASME J. Appl. Mech., **61**, pp. 777–783.
[24] Guest, S.D., and Pellegrino, S., 1996, "The Folding of Triangulated Cylinders—Part III: Experiments," ASME J. Appl. Mech., **63**, pp. 77–83.
[25] You, Z., and Cole, N., 2006, "Self-Locking Bi-Stable Deployable Booms," 47th AIAA/ASME/ASCE/AHS/ASC Structures, Structural Dynamics, and Materials Conference, Newport, RI, May 1–4, AIAA Paper No. 2006-1685.
[26] Zhang, X.W., Su, H., and Yu, T.X., 2009, "Energy Absorption of an Axially Crushed Square Tube With a Buckling Initiator," Int. J. Impact Eng., **36**(3), pp. 402–417.
[27] ABAQUS, 2007, ABAQUS Analysis User's Manual, Documentation Version 6.7, Dassault Systems Simulia Corp., Providence, RI.
[28] Ma, J., 2011, "Thin-Walled Tubes With Pre-Folded Origami Patterns as Energy Absorption Devices," Ph.D. thesis, University of Oxford, Oxford, UK.
[29] Wu, W., 2010, "Rigid Origami: Modelling, Application in Pre-Folded Cylinders and Manufacturing," Ph.D. thesis, University of Oxford, Oxford, UK.
[30] Abramowicz, W., and Jones, N., 1997, "Transition From Initial Global Bending to Progressive Buckling of Tubes Loaded Statically and Dynamically," Int. J. Impact Eng., **19**(5–6), pp. 415–437.
[31] Langseth, M., Hopperstad, O.S., and Berstad, T., 1999, "Crashworthiness of Aluminium Extrusions: Validation of Numerical Simulation, Effect of Mass Ratio and Impact Velocity," Int. J. Impact Eng., **22**(9–10), pp. 829–854.
[32] Meguid, S.A., Attia, M.S., Stranart, J.C., and Wang, W., 2007, "Solution Stability in the Dynamic Collapse of Square Aluminium Columns," Int. J. Impact Eng., **34**(2), pp. 348–359.
[33] Nojima, T., 2002, "Modelling of Folding Patterns in Flat Membranes and Cylinders by Origami," JSME Int. J., Ser. C, **45**(1), pp. 364–370.
[34] Nojima, T., 1999, "Modelling of Folding Patterns in Flat Membranes and Cylinders by Using Origami (in Japanese)," JSME, **66**(643), pp. 354–359.